



UNIVERSITY OF LEEDS

This is a repository copy of *Temperature response functions (G-functions) for single pile heat exchangers*.

White Rose Research Online URL for this paper:
<http://eprints.whiterose.ac.uk/104831/>

Version: Accepted Version

Article:

Loveridge, F orcid.org/0000-0002-6688-6305 and Powrie, W (2013) Temperature response functions (G-functions) for single pile heat exchangers. *Energy*, 57. pp. 554-564. ISSN 0360-5442

<https://doi.org/10.1016/j.energy.2013.04.060>

(c) 2013, Elsevier Ltd. This manuscript version is made available under the CC BY-NC-ND 4.0 license <https://creativecommons.org/licenses/by-nc-nd/4.0/>

Reuse

Unless indicated otherwise, fulltext items are protected by copyright with all rights reserved. The copyright exception in section 29 of the Copyright, Designs and Patents Act 1988 allows the making of a single copy solely for the purpose of non-commercial research or private study within the limits of fair dealing. The publisher or other rights-holder may allow further reproduction and re-use of this version - refer to the White Rose Research Online record for this item. Where records identify the publisher as the copyright holder, users can verify any specific terms of use on the publisher's website.

Takedown

If you consider content in White Rose Research Online to be in breach of UK law, please notify us by emailing eprints@whiterose.ac.uk including the URL of the record and the reason for the withdrawal request.



eprints@whiterose.ac.uk
<https://eprints.whiterose.ac.uk/>

Temperature Response functions (G-Functions) for Single Pile Heat Exchangers

Revision date: 21 February 2013

Words in main text: 6083

No figures 13

No tables 2+3

First author Fleur Loveridge^a

Second author William Powrie^b

a Research Fellow
Faculty of Engineering & Environment, University of Southampton

b Professor of Geotechnical Engineering and Dean of the Faculty
Faculty of Engineering & Environment, University of Southampton

Corresponding author Fleur Loveridge
Faculty of Engineering & Environment
Highfield, Southampton, UK, SO17 1BJ
Fleur.Loveridge@soton.ac.uk
0044 (0)7773346203

Temperature Response Functions (G-Functions) for Single Pile Heat Exchangers

Abstract

Foundation piles used as heat exchangers as part of a ground energy system have the potential to reduce energy use and carbon dioxide emissions from new buildings. However, current design approaches for pile heat exchangers are based on methods developed for boreholes which have a different geometry, with a much larger aspect (length to diameter) ratio. Current methods also neglect the transient behaviour of the pile concrete, instead assuming a steady state resistance for design purposes. As piles have a much larger volume of concrete than boreholes, this neglects the significant potential for heat storage within the pile. To overcome these shortcomings this paper presents new pile temperature response functions (G-functions) which are designed to reflect typical geometries of pile heat exchangers and include the transient response of the pile concrete. Owing to the larger number of pile sizes and pipe configurations which are possible with pile heat exchangers it is not feasible to developed a single unified G-function and instead upper and lower bound solutions are provided for different aspects ratios. (172 words)

Keywords: ground heat exchanger, pile, ground energy system, ground source heat pump system

Main Notation:

c	concrete cover to pipes (mm)
Fo	Fourier number (normalised time)
G	G-function or temperature response function
h_i	heat transfer coefficient (W/m^2K)
H	pile length (m)
n	number of pipes
q	heat transfer per unit depth of pile (W/m)
r	radius (m)
r_b	pile radius (m)
R	resistance (mK/W)
t	time (s)
T	temperature (K)
α	thermal diffusivity (m^2/s)
Δ	change in value
Φ	normalised temperature response
λ	thermal conductivity (W/mK)

Subscripts:

b	borehole or pile
c	pile concrete
f	fluid
g	ground
i	inner
o	outer
p	pipe

1 Introduction

Use of ground heat exchangers as part of a ground source heat pump system is an important means of reducing energy consumption in buildings. Traditionally the most commonly constructed type of heat exchangers are horizontal “slinky” type systems and deep boreholes. While horizontal systems are designed largely empirically, commercial software based on numerical and analytical methods is available for borehole heat exchangers. Recently there has been an increase in the use of building piled foundations as heat exchangers [1] as this can bring both material and carbon savings compared with the construction of special purpose deep boreholes. However, new design methods have not yet been developed for pile heat exchangers. Instead, methods developed for boreholes are typically applied, despite the different geometry of piles and boreholes. Geometrical differences are best captured by the aspect ratio (AR), which is the length (H) to diameter ($2r_b$) ratio of the heat exchanger. Piles typically have an AR of between 10 and 50, while for boreholes it may exceed 1000. In addition, large diameter piles offer opportunities for heat storage within the pile, something that established and emerging design methods neglect. Owing to these geometrical differences, optimal thermal efficiency is not necessarily being achieved for heat pump systems which use pile heat exchangers as the ground source.

1.1 Existing Design Approaches

It is now 25 years since Eskilson published his pioneering thesis [2] which presented so called G-functions for a range of borehole heat exchanger configurations. These functions give the normalised temperature (Φ) change of the ground at the edge of the borehole as a function of the Fourier number (or normalised time) resulting from a constant applied heat flux (q). It is assumed that the temperature is everywhere the same in the ground at the outset, and that the ground surface and far field conditions have a constant temperature equal to this initial value. The G-functions were developed by a combination of numerical and analytical means, assuming that the borehole is effectively a line heat source of finite length. The finite length is important, as the presence of a surface boundary condition of constant temperature leads to the development of a thermal steady state in the long term. Under these conditions, there is no further change in temperature for further input of heat at a constant rate. The time at which steady state occurs depends on the aspect ratio of the heat exchanger.

Eskilson [2] published a number of different g-function graphs showing the ground temperature response for a range of different borehole layouts, thus enabling the thermal interference between adjacent borehole heat exchangers to be taken into account. These G-functions now underpin a number of major commercial software packages which interpolate between pre-programmed g-functions according to the borehole configuration chosen by the designer. This accessible design approach has helped the adoption of borehole heat exchangers across many parts of the world, but especially northern Europe and North America. Some improvements have been made to the basic G-function concept since then; for example Bandos et al [3] have developed a method to include fluctuations in the ground surface temperature and the UK Partners in Innovation Project [4] developed software which allowed direct superposition of the single borehole G-functions in order to remove the need to interpolate between pre-programmed curves. However, the fundamental approach has remained unchanged.

As Eskilson's G-functions are based on a finite line heat source model, when they are applied to larger diameter pile heat exchangers they will underestimate the temperature change at smaller timescales [5]. Because of this, it is common to adopt a hollow cylindrical heat source model [6, 7] for pile heat exchangers. This model, first proposed by Ingersoll et al [6] and fully developed for ground heat exchanger applications by Bernier [7], is identical to the line source approach except that the source of the heat is assumed to be applied at the borehole or pile radius. The major disadvantage of this approach is that the cylindrical heat source is hollow; therefore all heat is assumed to flow outwards. However, recent work [8] has shown that for most pile heat exchangers the temperature response of the ground will fall somewhere between a line source model and the solid cylinder model of Man et al [9]. The latter is similar to the hollow cylindrical heat source approach, but critically assumes that heat can flow inwards from the heat source at the pile radius into the mass of the concrete as well as outwards into the ground. However, because none of these simple heat source models take into account the real geometry of pile heat exchangers (ie the particular arrangements of pipes within the pile concrete) none of them can fully characterise the early thermal behaviour.

In addition, the reduced aspect ratio of piles can be important. Field data for pile heat exchangers are rare, but a test plot of 300 mm diameter 10 m long piles was established by Wood et al [10]. Subsequent analysis showed discrepancies when attempting to predict the field fluid temperature results using software based on the finite line source model [11]. This was attributed by the authors to the short length of the piles. However, lack of similar high quality case studies for other pile geometries and pipe arrangements is problematic for validation of design methods. Recent instrumentation installed in the UK will contribute to increasing knowledge in this area [12].

Another disadvantage of current pile heat exchanger design approaches is that a simple heat source model, used to predict the temperature changes in the ground, is usually combined with the assumption that the pile itself is at steady state. This assumption allows a constant resistance to be used when calculating the temperature difference between the heat transfer fluid and the edge of the pile. This method has been adopted on the basis of its successful use in the design of borehole heat exchangers. However, pile heat exchangers can exceed 1m in diameter and therefore have a much larger area of concrete in their cross section. As a result they take much longer to reach steady state [13]. This means that to capture their early thermal behaviour appropriately, a constant resistance is no longer appropriate and a transient approach to the heat transfer in both the concrete and the ground should be taken.

Recently Li & Lai [14] have started to address these limitations by the development of G-functions based on superposition of infinite line sources in composite media. These two region analytical models are complex and the superposition must be derived for particular arrangements of pipes. They are also only applicable in the short term due to the infinite length of the heat source. G-functions are typically normalised with respect to thermal conductivity, and it is more difficult to normalise the temperature response function when there are two sets of thermal properties involved, ie the ground and the concrete. Li & Lai chose to normalise by the concrete conductivity, with the result that the gradient of the temperature response function will depend on the ground conductivity. This illustrates the difficulty of making a universal temperature response function for pile heat exchangers given the additional importance of the concrete behaviour to the overall performance of the pile.

Because of the complexities of pile heat exchanger geometries the problem is also well suited to numerical simulation. Codes developed for use with borehole heat exchangers, eg [15, 16] are equally applicable to pile applications. In addition, numerical methods may be used to couple the thermal and mechanical aspects of the pile behaviour [17]. This paper makes use of numerical solution of the diffusion equation to consider a wide range of pile heat exchanger geometries. We present new G-functions for pile heat exchangers based on empirical equations derived from extensive numerical simulations of a range of pile heat exchangers of different sizes and pipe arrangements. The G-functions can be viewed as an update to the previous works of Eskilson, taking into account typical pile heat exchanger geometries. Given the large number of variables which affect the performance of a pile heat exchanger it is not possible to develop a single universal G-function. Instead lower and upper bounds for different combinations of pile and pipe sizes and arrangements are presented so that the functions can remain as simple as possible. The new G-functions offer substantial improvement on existing solutions as they account for transient heat storage within the pile and are applicable over a full range of timescales. This is achieved by using separate G-functions for the temperature responses of the ground surrounding the pile (pile G-functions) and of the pile itself (concrete G-functions). As a lower and upper bound approach is adopted the new functions are also much simpler than the analytical solutions proposed by Li & Lai [14]. This means they can be readily and easily adopted into design software (an example using Matlab is presented later in the paper) and will be applicable to a far wider range of construction scenarios.

2 Ground Temperature Response Functions (Pile G-functions)

G-functions for pile heat exchangers are presented here as temperature response functions which provide a relationship between normalised temperature (Φ) and the Fourier number (Fo) for a constant rate of heat transfer q (W/m), where:

$$\Phi = \frac{2\pi\lambda_g}{q} \Delta T \quad (1)$$

$$\text{and } Fo = \frac{\alpha_g t}{r_b^2} \quad (2)$$

ΔT is the change in temperature, λ_g is the soil thermal conductivity, α_g is the soil thermal diffusivity and t is the elapsed time since application of the heat flux. The subscripts f and g will be used with Φ to denote the response of the fluid and the ground (at the pile radius where $r=r_b$) respectively.

The temperature response of the ground (Φ) is normalised by the soil thermal conductivity, λ_g , as is typical for the design of ground heat exchangers. The impact of the concrete thermal conductivity, λ_c , will be taken into account by consideration of the relative conductivities of the ground and the concrete. The temperature response of the concrete itself is discussed in Section 3.

2.1 Short Term Behaviour: 2D Simulation

Short term ground temperature response functions based on two dimensional numerical analyses have been presented in Loveridge et al [8] for a range of typical pile sizes and pipe arrangements (Table 1). The numerical models were constructed using the software COMSOL and comprise

horizontal slices through the pile and surrounding ground. As the simulation principally concerned the temperature changes occurring in the ground and concrete, and given that the pipes and fluid reach a thermal steady state rapidly, these elements were not included. Instead, a constant heat flux was applied to the boundary condition representing the outside of the pipes and the temperature changes due to conduction in the concrete and the ground were recorded. Full details of the numerical set up including meshing and boundary conditions are given in [8]. Two dimensional analysis is justified for timescales between $Fo=1$ and $Fo=10$ (depending on the accuracy required) as the pile end effects are not yet significant. The inclusion of three dimensional effects will be discussed in Sections 2.2 & 2.3.

Based on average temperatures around the pile circumference, a summary of the model ground temperature responses, plotted as Φ_g against normalised time, Fo , is presented in Figure 1. A range of curves is possible depending on the number and arrangement of the heat exchanger pipes, the size of the pile and the relative properties of the pile concrete and the surrounding ground. Typically the responses lie between two analytical solutions:

1. The simplified line source (Equation 4), where the exponential integral in Equation 3 is replaced by a log-linear relationship:

$$\Phi = \frac{1}{2} Ei \left[\frac{1}{4Fo} \right] \quad (3)$$

$$\Phi \approx \frac{1}{2} [\ln(4Fo) - \gamma] \quad (4)$$

2. The solid cylinder solution [9], which when simplified becomes:

$$\ln \left(\frac{\Phi}{2} \right) = -2.321016 + 0.499615 \ln(Fo) - 0.027243 [\ln(Fo)]^2 - 0.00525 [\ln(Fo)]^3 + 0.000264311 [\ln(Fo)]^4 + 0.0000687391 2[\ln(Fo)]^5 \quad (5)$$

The hollow cylinder model, commonly used for boreholes, was found to be less appropriate for representing pile heat exchangers.

Table 1 Pile heat exchanger geometries and range of properties used in the 2D Model

Pile Diameter	Pipe External Diameter	Number of Pipes	Pipe Positions (see note)	Ground and Concrete Conductivity	Ground and Concrete Volumetric Heat Capacity
300 mm	25 mm	2	Edge – 50 mm cover	1 W/mK or 2 W/mK	1.6 MJ/m ³ K
			Central – 105 mm cover		
600 mm		4	Edge – 75 mm cover		
			Central – 255 mm cover		
1200 mm		8	Edge – 75 mm cover		
		4	Central – 555 mm cover		

Note: cover is the amount of concrete between the pipes and the ground; centrally placed pipes are assumed to be symmetrically placed around a 40mm diameter steel bar.

Figure 1 – Range of short term pile temperature response functions for the cases given in Table 1 (based on 2D numerical simulations by Loveridge et al [8])

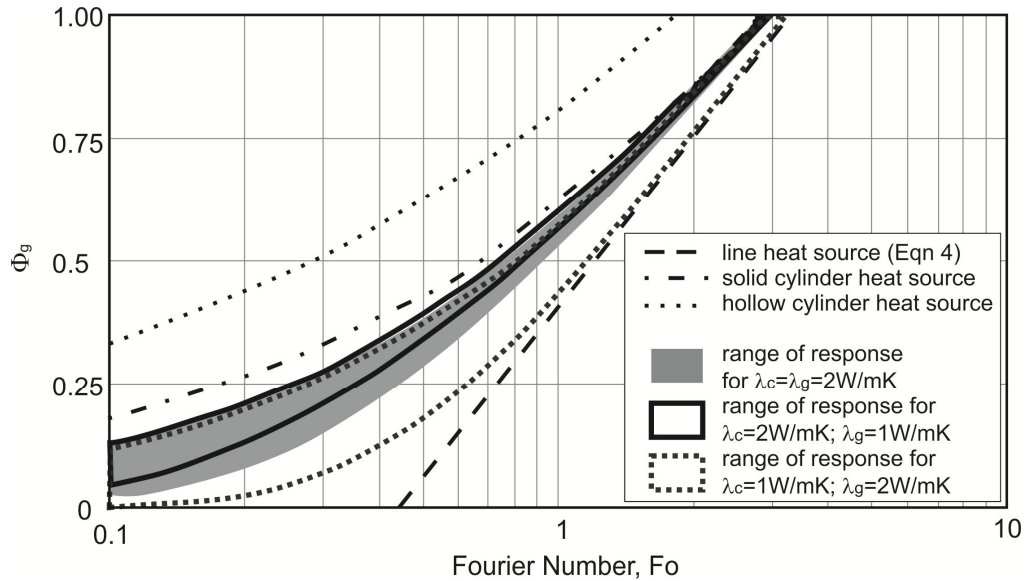


Table 2 Upper Bound (UB) and Lower Bound (LB) temperature responses as for the cases shown in Table 1 and Figure 1.

	Pile Diameter, $2r_b$	Number of Pipes, n	Concrete cover, c	Concrete conductivity	Concrete volumetric heat capacity	Ground conductivity	Ground volumetric heat capacity
UB	1200 mm	8	75 mm cover	2 W/mK	1.6 MJ/m ³ K	1 W/mK	1.6 MJ/m ³ K
LB	1200 mm	4	555 mm cover	1 W/mK	1.6 MJ/m ³ K	2 W/mK	1.6 MJ/m ³ K

Ground temperature responses are closest to the line source solution (Equation 4) when the pipes are positioned in the centre of the pile, and closest to the solid cylinder model (Equation 5) when the pipes are nearer the pile edge. When the concrete conductivity is less than that of the ground, the response will move closer to the line source; when the reverse is true the response tends to move closer to the solid cylinder solution. The results for smaller diameter piles tend to be positioned more centrally between the line source and solid cylinder solutions, while larger diameter piles have a more varied response. Consequently both the lower and upper bound responses are given by larger diameter piles, as summarised in Table 2.

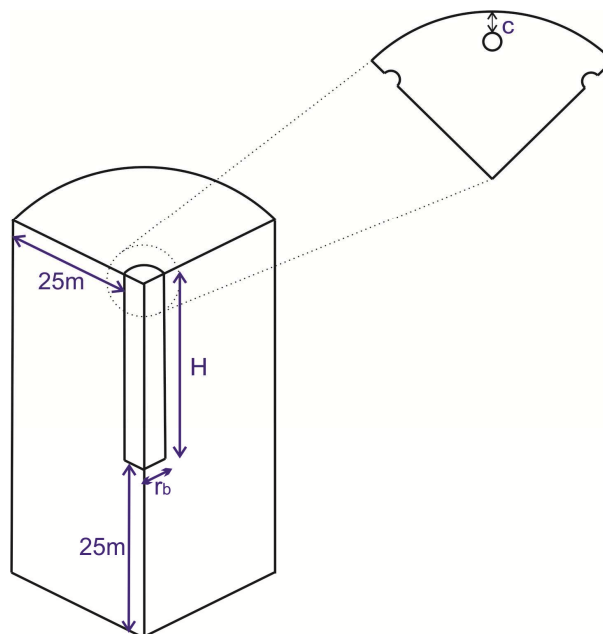
2.2 Long Term Behaviour: 3D Simulation

In the longer term full three dimensional simulations are required in order to determine the temperature response functions for pile heat exchangers. This is because the short length of most piles means that the ground surface boundary condition will rapidly start to influence the results. In the very long term the temperature response will converge towards that of other existing analytical

solutions: the finite line source, fine solid cylinder and finite hollow cylinder all become equivalent as Fo becomes large (typically greater than 100). To confirm the thermal behaviour of pile heat exchangers over intermediate timescales a three dimensional model was set up using the finite element software ABAQUS in heat conduction mode. To reduce the number of simulations required, only the upper and lower bound scenarios (refer to Table 2) identified in Section 2.1 were developed into full three dimensional models. While more extreme scenarios could possibly be found, the conditions presented in Figure 1 are intended to represent the range of conditions likely to be encountered in most practical scenarios. As the temperature response will be affected by the surface boundary, different aspect ratios have been considered for both the upper and lower bound cases. Based on previous studies of constructed pile heat exchangers [5], aspect ratios of 15, 25, $33\frac{1}{3}$ and 50 have been used.

The model is based around a quarter cylindrical sector (Figure 2), taking account of symmetry to reduce the size of the model. A constant rate of heat flux is applied at the pipe boundaries; the temperature response at these boundaries and at the edge of the pile is calculated by the model. The pipes themselves were not modelled, so that any thermal resistance associated with the pipe or the fluid was not included in the model. This is considered appropriate as this element of the heat transfer process will reach steady state rapidly and is also straightforward to calculate by other means (refer to Section 4.14.1). The model contains the ground surrounding the pile up to a radial distance of 25 m and beneath the base of the pile to the same distance. Sensitivity analyses have shown that this is appropriate for times up to $Fo=200$.

Figure 2 Schematic of three dimensional model for $Fo < 200$ (detail shown for upper bound case)



The soil and concrete properties used in the model are given in Table 2. The properties were assumed to be constant throughout the simulations and are not subject to change with temperature. This is considered appropriate for the relatively small temperature changes associated with ground energy systems. The lines of symmetry in the model were insulated, while the outer

radial edge, along with the top and base, are kept at a constant temperature of zero degrees. The initial temperature everywhere in the model was also zero degrees so that the model output provided a direct change in temperature values at any given point. No groundwater flow, or other external influence on heat flow, was permitted.

The model was meshed using 8 node linear heat transfer brick elements. Element sizes were adjusted to balance accuracy of results and analysis run times. The results were verified in two ways. Short time outputs were compared to the response functions presented in Loveridge et al [8] while the final temperature changes at $Fo=200$ were compared to the results of existing finite line and finite cylinder source models. In all cases the average temperature (both in terms of circumferential and vertical variation) at the pile edge was used by taking the mean of the calculated temperatures at all the nodes forming the circumferential surface of the pile. Normalised temperatures were typically within 0.005 of the known solutions, which is equivalent to temperature differences of no more than 0.01 degrees.

For the largest values of Fo (typically $Fo>100$), the upper and lower bound pile scenarios are equivalent and standard finite line source methods have been used to calculate the steady state section of the temperature response functions for the four different aspect ratios.

2.3 Simulation Results

Figures 3 and 4 show the results of the three dimensional model plotted as average ground temperature response functions for four different aspect ratios for the upper and lower bound pile scenarios respectively. Also shown are the upper and lower bound short term responses from the two dimensional model. Differences between the two dimensional and three dimensional cases first appear after $Fo=1$, becoming significant (up to 10% to 15%) by $Fo=10$. These differences are greatest for smaller aspect ratio piles. Although not shown for clarity, by $Fo=100$ the model results have converged with Eskilson's finite line source.

Combining the results from the 2D and 3D models and the finite line source, the overall average temperature response functions for pile heat exchangers are given in Figure 5. Eight separate curves are required to characterise the response: four aspect ratios for each of the upper and lower bound solutions. For times up to approximately $Fo=10$ the temperature response is controlled by the pile internal geometry (size, number and arrangements of pipes). At this time only two curves are distinguishable: the upper and lower bound, as the aspect ratio does not yet influence the temperature response significantly. At larger values of Fo , the upper and lower bound curves plot on top of each other, but diverge according to the pile aspect ratio (effectively the pile external geometry). Therefore effectively only four curves are visible at larger values of Fo .

The upper bound solutions typically apply to cases where the heat transfer pipes are installed close to the edge of the pile cross section, with larger diameter piles being closest to the upper bound. The lower bound solutions typically apply to cases where the pipes are installed in the centre of the pile. Again larger diameter piles are more likely to be closer to the bound, with smaller diameter piles falling between the upper and lower bounds. It is important to note that there is no significant straight line portion of the temperature response curves in Figure 5. This means that the flow is never purely radial as assumed in some simpler models.

To allow for easier implementation of the temperature response functions a curve fitting exercise has been carried out for the eight G-functions presented in Figure 5, the results of which are contained in Appendix A.

Figure 3 Average ground temperature response from 3D model (upper bound)

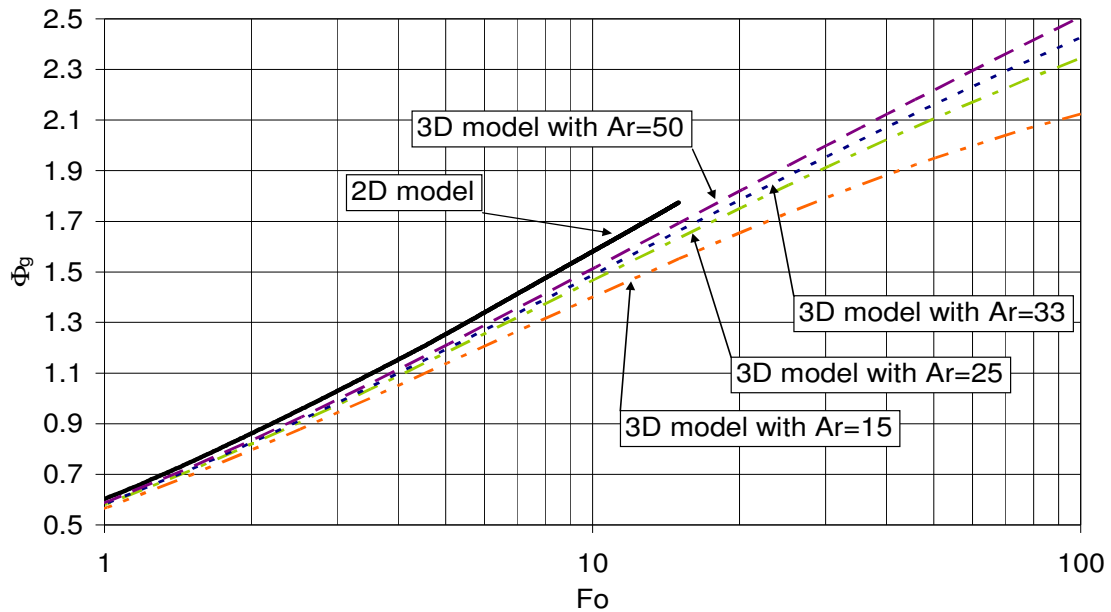


Figure 4 Average ground temperature response from 3D model (lower bound)

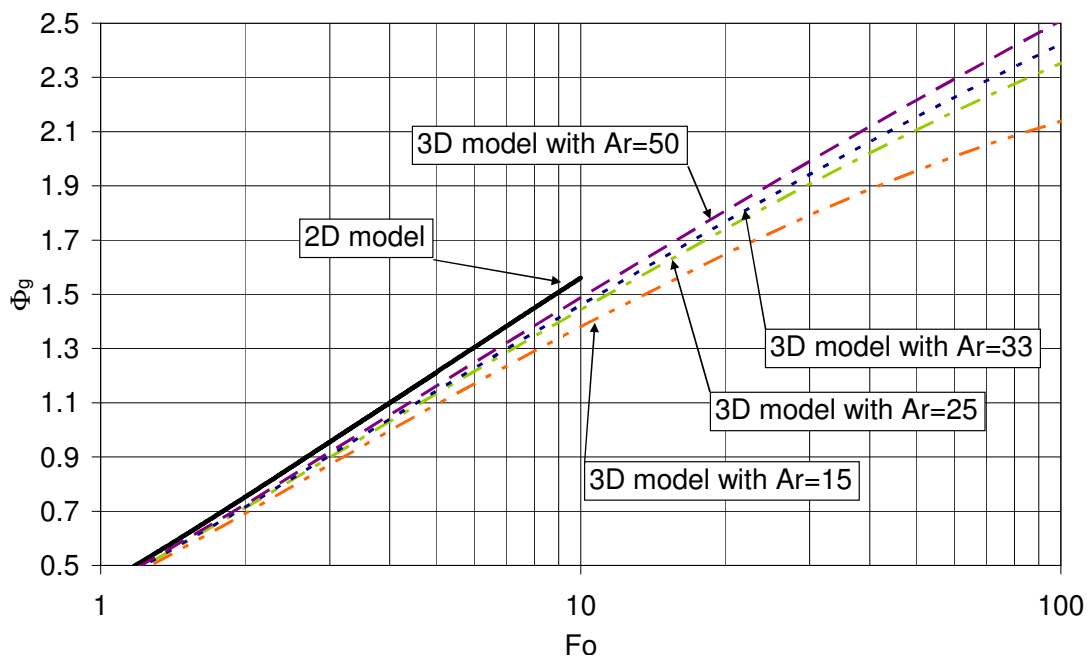
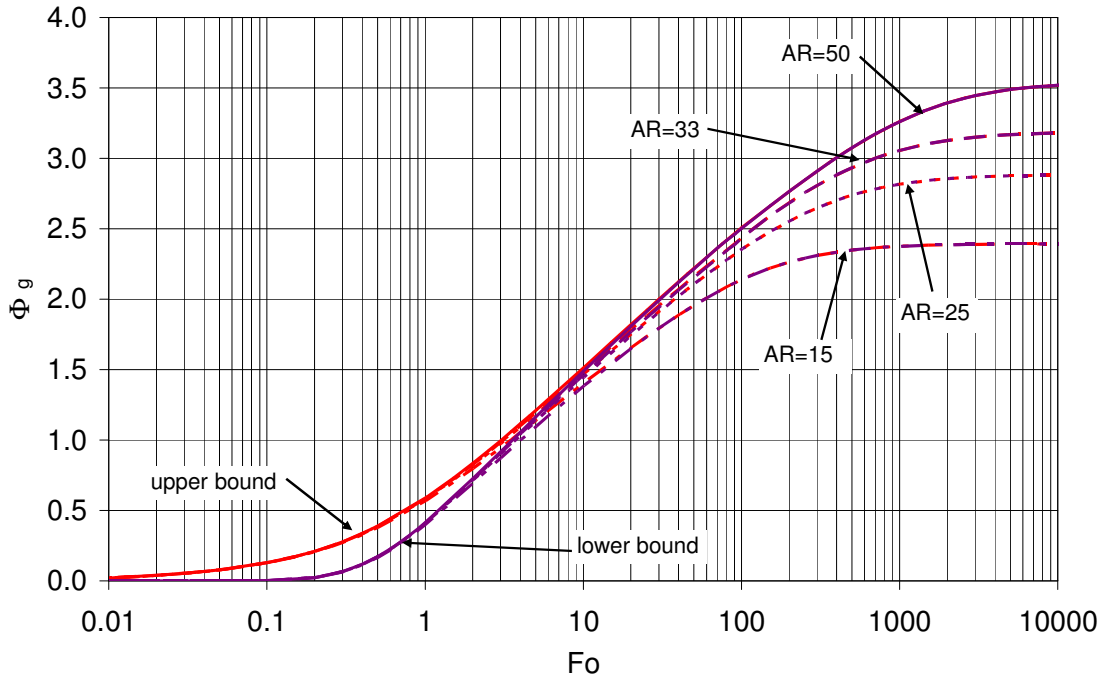


Figure 5 Pile heat exchanger G-functions



3 Transient Thermal Resistance of the Pile (Concrete G-functions)

To incorporate the transient response of the pile concrete into the overall temperature response function, the proportion of the steady state thermal resistance that has been achieved at a given value of Fo has been calculated using the output from the 2D model. As 90% to 95% of the steady state in the concrete is reached by $Fo=1$, this 2D simplification is considered appropriate. At any given time the thermal resistance of the concrete part of the pile is calculated according to Equation 6:

$$R_c = \frac{\overline{T}_p - \overline{T}_b}{q} \quad (6)$$

where \overline{T}_p and \overline{T}_b are the integral mean values of the temperature at the pipes and the pile edge boundaries respectively, and q is the total heat flux applied to the all the pipe boundaries. The steady state resistance is the asymptotic value of Equation 6 calculated at larger values of time, typically when Fo approaches 10. Thus at any point in time the transient value of R_c can be compared with the steady state value. A summary of the results of these calculations is shown in Figure 6 and Figure 7. As the response is specific to the pile construction and cannot be generalised into a single universal response curve, pairs of upper and lower bound solutions have been developed for the cases where the pipes are in the centre and near the edge of the pile respectively. The two cases have been treated separately as, especially for larger diameter piles, the shapes of the curves are different. In all cases the upper bound solutions represent the case of a large pile where the ground is less conductive than the pile concrete. The lower bound represents the opposite situation, with a small pile and the ground being more conductive than the pile. To allow these

response curves to be implemented as concrete G-functions, curve fit data for Figures 6 and 7 are presented in Appendix B.

Figure 6 Concrete G-functions: proportion of steady state thermal resistance as a function of Fo (pipes placed centrally)

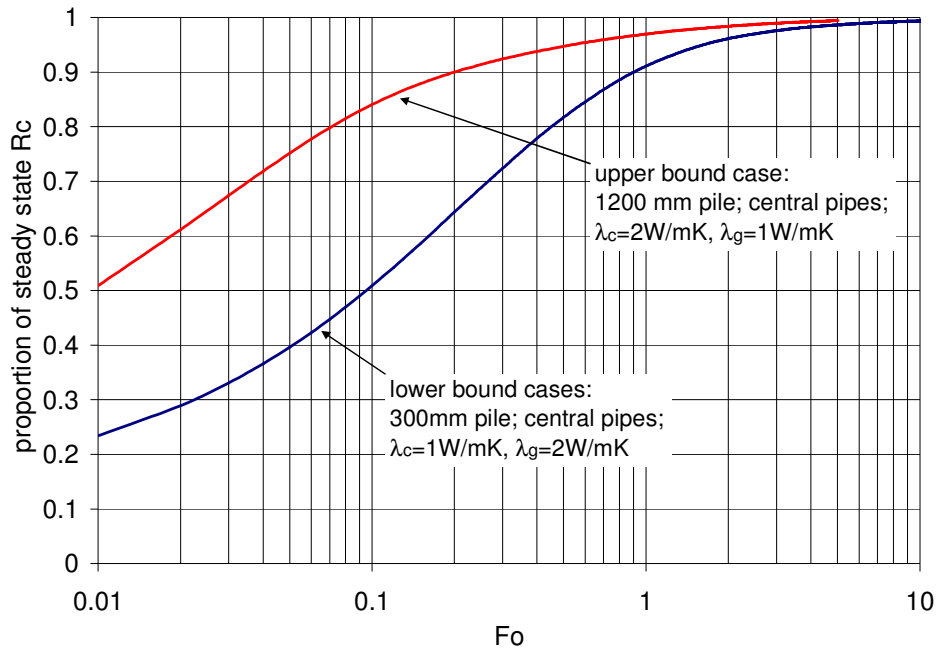
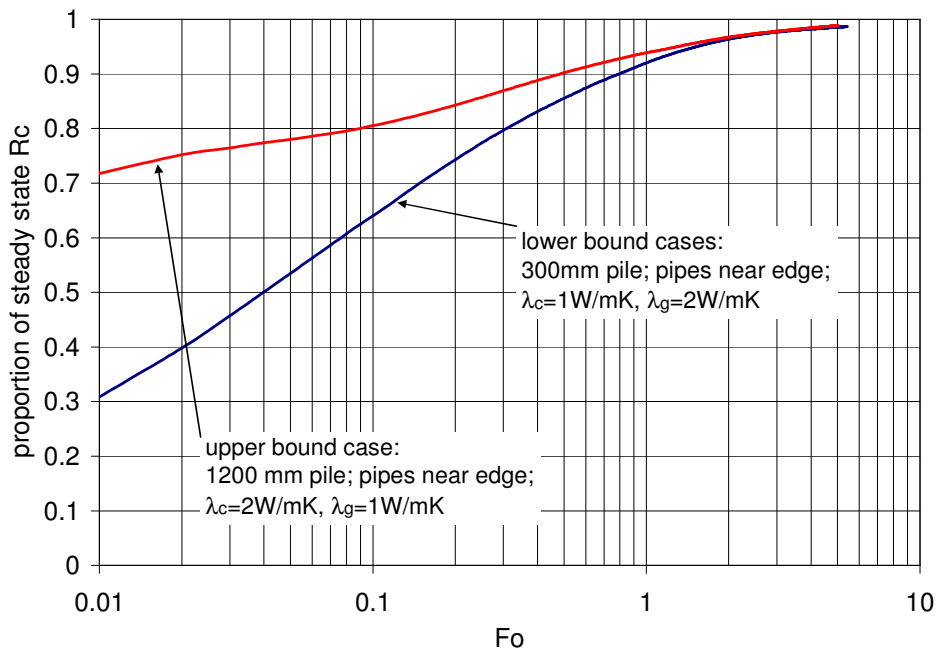


Figure 7 Concrete G-functions: proportion of steady state thermal resistance as a function of Fo (pipes placed near the pile edge)



4 Calculating the Fluid Temperature Response using New Pile and Concrete G-functions

To determine the overall temperature response function of a pile heat exchanger, three elements must be considered:

1. The thermal resistance of the pipes and fluid
2. The transient pile concrete response
3. The ground response

Thus:

$$\Delta T_f = qR_p + qR_c G_c + \frac{q}{2\pi\lambda_g} G_g \quad (7)$$

where q is the heat transfer rate per metre length of the pile heat exchanger, R_p is resistance of the pipes (including the fluid), G_c is the concrete G-function describing the transient concrete response and G_g is the pile G-function for the transient response of the ground surrounding the piles.

4.1 Pipe Resistance

R_p can be defined as the sum of the pipe conductive resistance and the pipe convective resistance as follows:

$$R_p = R_{pconv} + R_{pcond} \quad (8)$$

The convective resistance is then:

$$R_{pconv} = \frac{1}{2n\pi r_i h_i} \quad (9)$$

where n is the number of pipes within the heat exchanger cross section, r_i is the pipe internal radius and h_i is the heat transfer coefficient. The latter can be calculated using a number of standard equations such as the Dittus-Boelter equation [18] or the Gnielinski correlation [19]. The pipe conductive resistance can be assessed using the equation for the resistance of a hollow cylinder, which for n pipes in parallel gives:

$$R_{pcond} = \frac{\ln(r_o/r_i)}{2n\pi\lambda_{pipe}} \quad (10)$$

where r_o is the outer radius of the pipe.

4.2 Pile Concrete Resistance

The resistance of the concrete part of the pile, termed R_c , can be calculated numerically as per Equation 6, or analytically by the complex multi-pole method [20]. Alternatively, simpler empirical equations for determining R_c are available [13]. For the special case of a pile with only two pipes in the cross section, the multi-pole method becomes easier to apply. The first order multipole and related line source equations for the two pipe case are presented by Hellstrom [21].

4.3 Pile and Concrete G-Functions

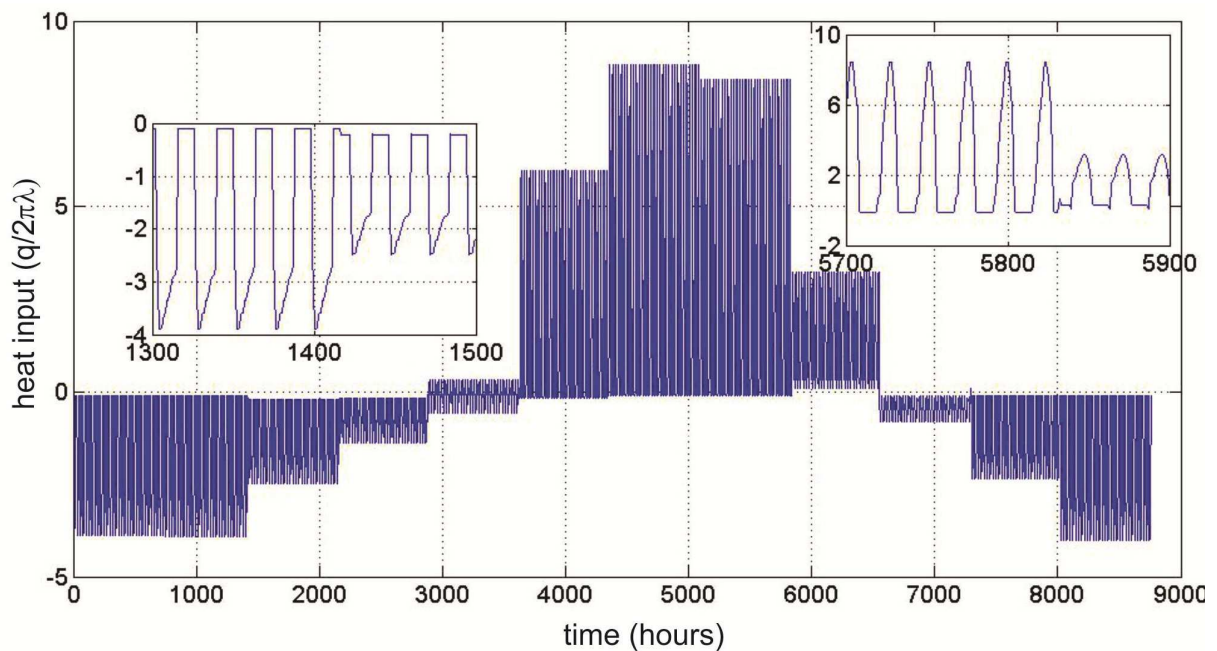
The new G-functions are presented in Figures 5, 6 & 7. For easier implementation in analysis, empirical equations for the curves have been calculated by a least squares regression, using approximately equal periods of $\ln(\text{Fo})$. Equations for G_g are given in Appendix A and depend on the pipe arrangements and the pile aspect ratio respectively. Equations for G_c ($\text{Fo} < 10$) are given in Appendix B according to the pile size and pipe arrangements. For $\text{Fo} > 10$ the pile concrete is at steady state and G_c can be taken to equal 1.

5 Example Applications

5.1 Controlled Energy Input

To demonstrate the application of the new G-functions and to highlight the differences between this and existing design equations, an example thermal load profile has been used to calculate the ground and fluid response for a number of different cases. The calculations are carried out for a 600 mm diameter, 20 m long pile heat exchanger ($\text{AR} = 33 \frac{1}{3}$) with a thermal conductivity of $\lambda_c = 1 \text{ W/mK}$. The surrounding ground is assumed to have thermal properties described by $\lambda_g = 2 \text{ W/mK}$ and $\alpha_g = 1 \times 10^{-6} \text{ m}^2/\text{s}$. The pile concrete thermal resistance R_c is 0.075 mK/W and the pipe resistance R_p is 0.025 mK/W for four pipes placed near the edge of the pile. The building thermal load profile for a typical year has been developed from a numerical simulation of a modern multi-use development in the South East of England, scaled down to an appropriate level for a single pile. The profile, shown in Figure 8, includes heating and cooling loads, and has been used as hourly input data with changes in load on daily cycles.

Figure 8 Example thermal loads for one year commencing in autumn (insets shows daily cycle detail)



Note: positive thermal loads are heat injection to the ground (building cooling); negative thermal loads are heat extraction from the ground (building heating)

5.1.1 Ground Temperature Response Functions

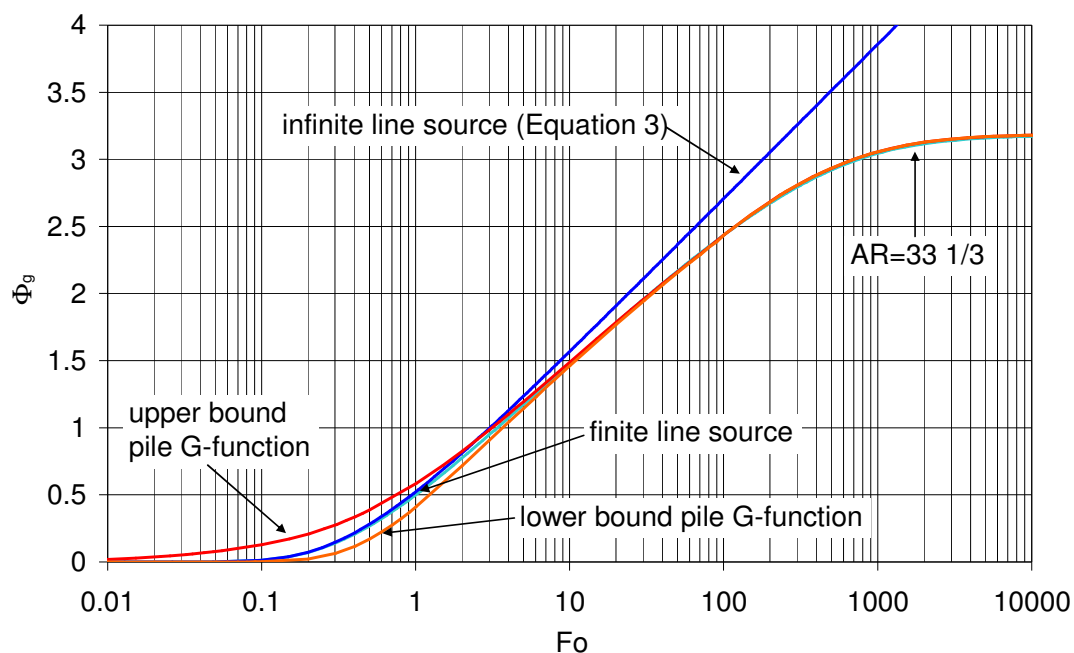
Using these input parameters, the temperature change in the ground has been calculated for a one year period for the following ground temperature response functions (Figure 9):

1. An infinite line source (using the exponential integral, Equation 3)
2. A finite line source [2] with $AR=33^{1/3}$
3. An upper bound pile G-function (Equation A-1) with $AR=33^{1/3}$
4. A lower bound pile G-function (Equation A-2) with $AR=33^{1/3}$

Functions 1 and 2 represent those regularly used in current practice. The hollow cylinder is also used in some commercial software, but as discussed this is not considered appropriate and therefore has been discounted in this example. Functions 3 and 4 are the new G-functions proposed by this study. For clarity of subsequent presentation the solid cylinder model [9] has not been used as this would be close in behaviour to the proposed upper bound solution. The two-zone analytical solutions of Li & Lai [14] has not been used in this comparison as the results should be equivalent to the upper and lower bound pile G-functions if calculated for the same pipe positions and soil and concrete parameters. However, the complexity of these functions does not make them attractive to routine implementation.

It should also be noted that when using the full analytical form of the infinite line source (Equation 3) rather than the mathematical simplification (Equation 4), then the line heat source plots between the upper and lower bound pile G-functions (Figure 9). This is because Equation 3 is representative of the case where the ground and concrete conductivity are equal and the pipes are in the centre of the pile. This is the equivalent of the lower part of the range of responses for $\lambda_c=\lambda_g$ as shown in Figure 1.

Figure 9 Temperature response functions used in the example calculations



To include the hourly fluctuations in applied thermal load, q , superposition has been applied to the thermal load time series according to the following equation:

$$\Delta T_n = \sum_{i=1}^{i=n} \frac{q_i}{2\pi\lambda_g} [G(Fo_n - Fo_{(i-1)}) - G(Fo_n - Fo_i)] \quad (11)$$

where n is the point in normalised time in which the superposition is evaluated and G is the G-function (one of the cases 1 to 4 above) calculated at the value of Fo prescribed in the equation. Equation 11 has been coded in the software Matlab to allow calculation of the sum in hourly timesteps for the period of one year.

Figure 10 Differences in temperature response for a finite and infinite line source model: a) over one year; b) minimum temperatures during heat extraction; c) maximum temperatures during heat injection

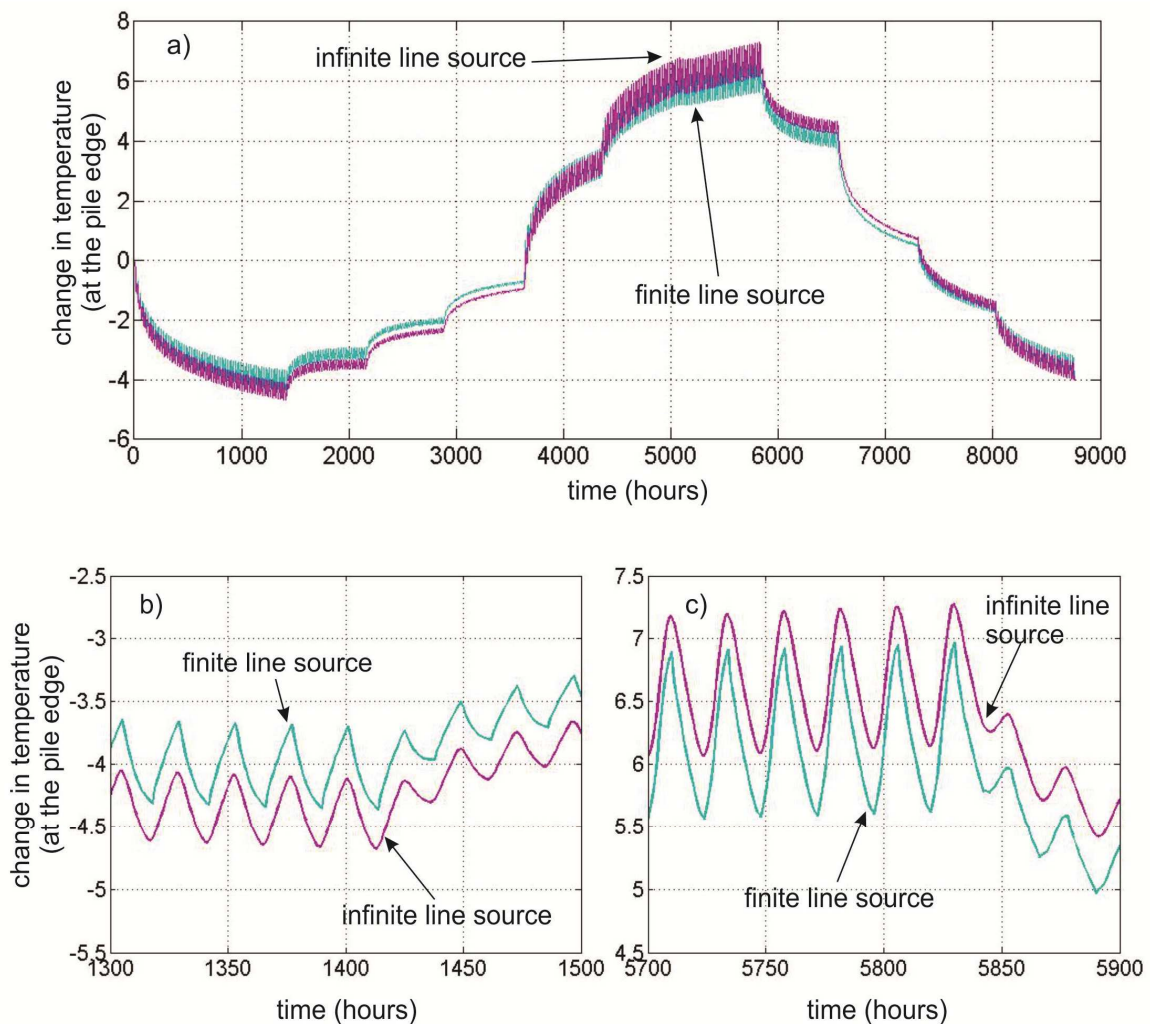
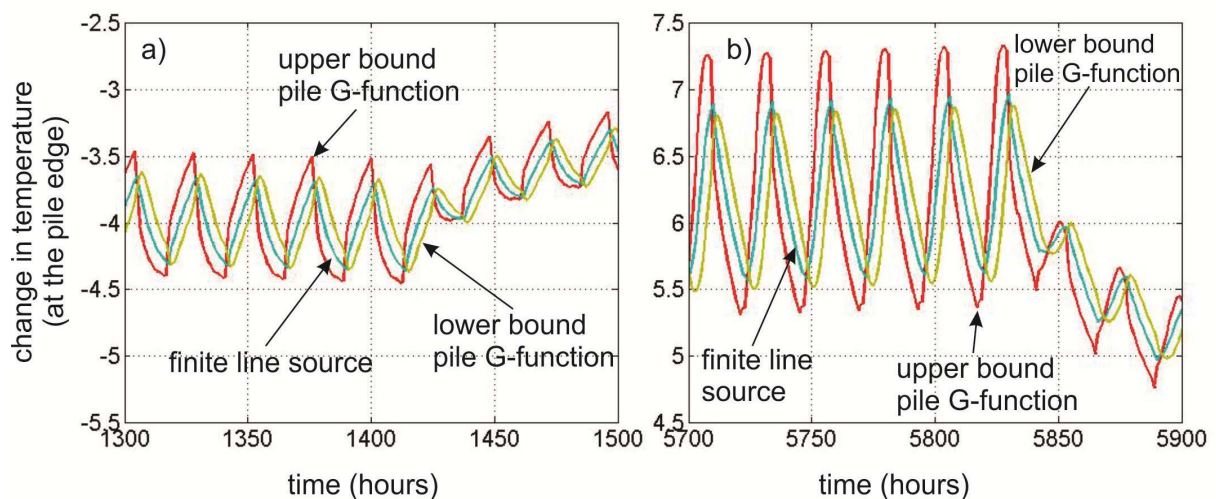


Figure 10 shows the calculated temperature changes in the ground for the infinite and finite line source. Figure 10a presents the data for the entire year and shows that the peak temperatures do not always correspond exactly with the peak thermal loads owing to the cumulative effect throughout the year. Figures 10b and 10c show the results in more detail for the periods when the calculated temperature changes are greatest. This illustrates the importance of taking into account

the finite length of a pile heat exchanger, even for an operational period as short as one year. It can be seen that the infinite line source always overestimates the extreme temperatures in summer and winter, with the finite line source providing a smaller range of calculated temperature changes. Thus, while the infinite line source may be conservative in predicting temperature change, it does not offer the most energy efficient design solution. This effect will be more significant for smaller aspect ratio piles and for unbalanced thermal loads over longer time periods.

The subsequent figures show comparisons between the other temperature response functions listed above. They all show the same overall pattern of temperature change, but with important differences concerning the calculated minimum and maximum temperature changes. Therefore, for clarity, only the minimum and maximum temperature changes are shown in the following figures, equivalent to parts b and c of Figure 10. Figure 11 shows the difference in temperature response according to the idealised geometry of the pile, ie whether an upper bound, lower bound or line source is chosen to represent the pile and pipe arrangements. In all cases the finite length of the heat exchanger is accounted for (ie response functions 2, 3 & 4 are compared). The upper bound pile G-functions shows a greater range of temperature changes than the lower bound pile G-function and the finite line source. This is especially the case during the middle part of the year (summer) when the magnitude of the heat injection peaks are particularly high (Figure 8) and greater in magnitude than the corresponding daily heat extraction peaks in winter. The lower bound and line source solutions also show greater lag in response time with smaller more damped responses to the heat input compared with the upper bound. The calculated temperature difference between the different functions is up to approximately 0.5°C.

Figure 11 Differences in temperature response for the pile G-functions compared with a finite line source model: a) minimum temperatures during heat extraction; b) maximum temperatures during heat injection



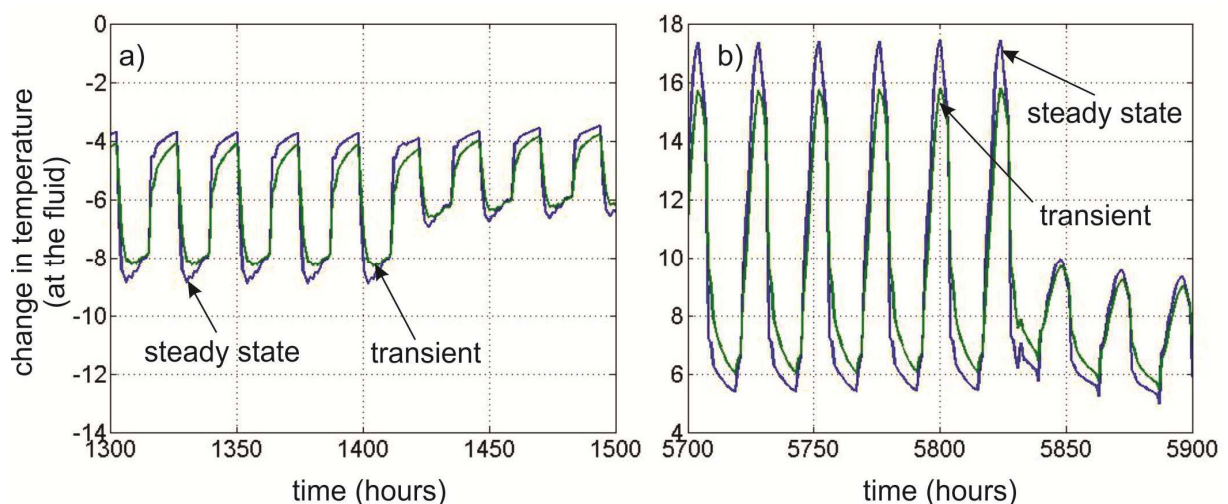
It is also worth noting that the hollow cylinder model, which although not compared directly in these analyses, is known to predict greater temperature changes than the upper bound pile G-function (Figure 1). Like the use of the infinite line source, this would also provide a conservative alternative solution for predicting temperature changes around pile heat exchangers. However, the differences

shown in Figure 1 would be exacerbated for small timescale changes in heat flux and thus this approach is not recommended.

5.1.2 Concrete G-functions

The most important difference in the calculated temperature changes between existing methods and the proposed new G-functions occurs when the contribution of the pile concrete is included in the calculations. Figures 10 and 11 only consider the temperature change in the ground, ie just the third term in Equation 7. The overall fluid temperature response is calculated by applying Equation 7 in full, using superposition to consider the transient response of the pile concrete. Figure 12 compares an upper bound pile G-function where a steady state is assumed in the pile concrete (ie $G_c=1$) with the case where transient behaviour is taken into account by use of a concrete G-function (equation B-1). In this case lower bound conditions for the concrete have been assumed. Generally, use of steady state resistance for the pile concrete ($G_c=1$) will overestimate the range of temperature response. This means that there are missed opportunities to improve the system efficiency during design. For the example thermal loads analysed, there is a temperature difference of up to 2°C between the steady and transient approaches in the summer and a smaller 1°C temperature difference in winter. Greater differences would be expected in cases where the hourly variations of thermal loads are most extreme. Also worth noting is that the inclusion of the concrete within the model gives a much wider range of calculated temperatures, with the fluid temperature change ranging from -9°C to +18°C, compared with the ground temperature changes which are only -4.5°C to +7.5°C. This reflects the important, yet often underestimated role, of the pile concrete in the overall heat transfer and storage around pile heat exchangers.

Figure 12 Differences in temperature response for upper bound pile G-functions using steady state and transient approaches to the pile concrete: a) minimum temperatures during heat extraction; b) maximum temperatures during heat injection



5.2 Controlled Temperature Range

The analysis above demonstrates that for the example scenario use of the new concrete G-function results in a calculated temperature change range which is 3°C less than the case where a constant steady state R_b is applied. To translate this temperature difference into energy savings the reverse problem is analysed. This is more realistic of real operation, where typically temperature limits are

applied to the fluid as it enters and leaves the heat pump and the aim of design is to maximise the amount of energy which can be extracted from, injected into or stored within the ground, while not exceeding those limits.

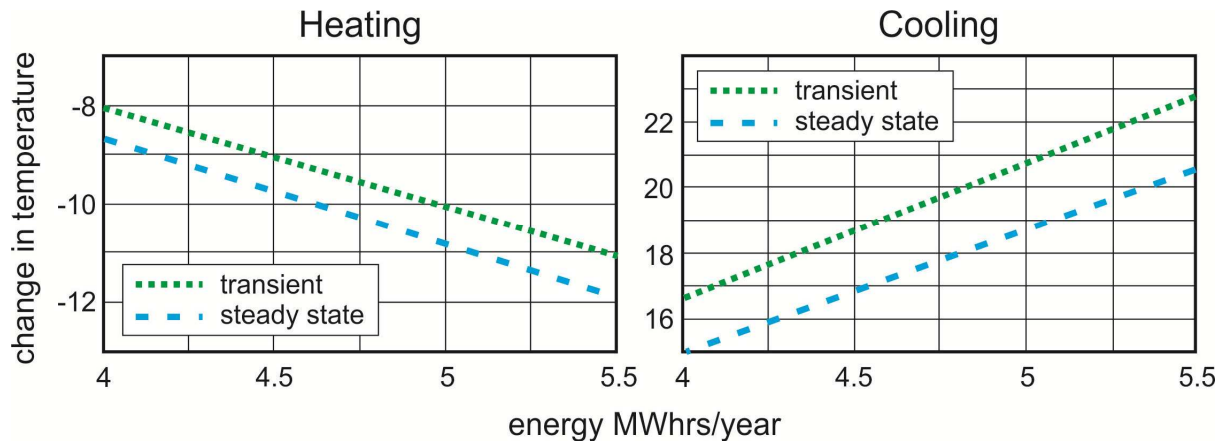
The same scenario as the above example is used, with a 600 mm diameter, 20 m long pile heat exchanger ($AR=33^{1/3}$) with a concrete thermal conductivity of $\lambda_c=1$ W/mK. The surrounding ground is assumed to have thermal properties described by $\lambda_g=2$ W/mK and $\alpha_g=1 \times 10^{-6}$ m²/s. The pile concrete thermal resistance R_c is 0.075 mK/W and the pipe resistance R_p is 0.025 mK/W for four pipes placed near the edge of the pile. Assuming a typical initial ground temperature of 12°C, temperature limits are specified at 2°C and 32°C (ie changes of -10°C and +20°C). Two cases are considered: the upper bound pile G-function where a steady state is assumed in the pile concrete (ie $G_c=1$) with the case where transient behaviour is taken into account by use of a concrete G-function (equation B-1). The traditional finite line source is not considered in this example. Although this approach would result in a smaller quantity of energy being calculated compared to the upper bound pile G-function, the difference is secondary compared to the differences between the transient and steady state approach to the pile concrete.

For simplicity, both of calculation and of presentation of the results, the amount of energy obtainable between these temperature limits has not be absolutely maximised. Instead, the shape of the respective heating and cooling demand curve (Figure 8) has been maintained, but the power input at each of the hourly time steps has been increased by an equal amount pro rata. The total annual energy input represented by Figure 8 is 4115 kWhrs/yr heating and 4224 kWhrs/yr cooling. These figures are the contribution of one pile heat exchanger, whereas in a real system many pile heat exchangers would be working together to provide a meaningful contribution to the building heat and cooling demand.

Figure 13 shows the relationship between the available energy and the specified fluid temperature limits for the two cases under consideration. The greater the temperature limits the greater the energy obtainable from the ground. For the temperature limits specified (-10°C and +20°C) the difference in available energy between the steady state and transient (concrete G-function) cases are approximately 350 kWhrs/year and 525 kWhrs/year in heating and cooling respectively. These figures refer to a single pile. This amounts to respectively 8% and 10% increases in available energy when the concrete G-function is used compared to the traditional steady state approach.

For the example considered, the improvement is greatest in the case of cooling, or heat injection to the ground. This is because the cooling loads change more rapidly compared to the heating loads (refer to Figure 8). The greater the short term fluctuations in thermal load the more important it becomes to consider the transient behaviour of the pile concrete, effectively the short term storage of energy in the concrete. In this example energy storage totals approximately 0.9 MWhrs/year per pile. For larger diameter piles or where the short terms fluctuations in thermal loads are greater this figure would be substantially increased. The use of an infinite line source (refer to Figure 10) or a finite line source (refer to Figure 11) instead of an upper bound pile G-function would also underestimate the energy available.

Figure 13 Relationship between allowable fluid temperature change and available energy for example single pile heat exchanger: a) heating; b) cooling



Note: refer to text for details of pile and thermal load scenarios considered

5.3 Discussion

The calculation results presented in Figures 10, 11, 12 and 13 are examples based on particular pile properties and thermal loading conditions. Some of the differences between the results obtained using pile and concrete G-functions and those using traditional line source approaches are small, while others are significant. Under-predicting temperature ranges as shown in Figure 12 would lead to a reduction in the assessed energy capacity of the system as demonstrated in Figure 13. This is because systems must operate within defined temperature limits and use of a steady state pile resistance would suggest that less heat transfer is possible within any given limits. In this context, 3°C is significant, representing 0.9 MWhr/year for a single heat exchanger. This aspect of behaviour is especially true for pile heat exchangers for two reasons. First they must be operated across smaller ranges of temperatures than borehole heat exchangers to remove any risk of ground freezing at low temperatures. Secondly, they also contain a much larger volume of concrete in their cross section.

The actual impact of the differences between implementing pile and concrete G-functions compared with traditional methods will depend on the particular scheme details. However, based on the underlying equations it can be inferred that benefit from using pile and concrete G-functions will be greatest when:

1. There is a lower bound condition with respect to transient behaviour of the pile concrete. This would occur in situations where the pile concrete is less conductive than the ground.
2. Piles are of larger diameter. Although larger diameter piles are associated with the upper bound concrete G-functions, the pile diameter is a non-dimensioning variable for the Fourier Number, Fo . This means that a one hour time step for larger diameter piles will be equivalent to a much smaller value of Fo and hence a lesser proportion of steady state in the pile.
3. Thermal load scenarios are such that there are significant changes in applied heat flux over small timescales, especially when the overall applied thermal load is also large. It is in these scenarios that heat storage in the pile will be most significant.

4. In long term analyses where there is a net imbalance of heat transfer with respect to heat injection and heat extraction.

6 Conclusions

New G-Functions for pile heat exchangers have been presented, split into pile G-functions which describe the temperature changes in the ground and concrete G-functions which describe the temperature changes within the pile itself. The functions capture the short term variation in behaviour depending on the internal pipe arrangements and the material thermal properties in addition to the transient heat transfer and storage within the pile concrete. At larger timescales Eskilson's G-functions, based on a finite line source, are appropriate. As the short and long term behaviour depends on the internal and external geometry respectively, it has not been possible to develop a single unified G-function for all pile heat exchangers. Instead, lower and upper bound solutions have been presented which can be combined according to the specific circumstances under consideration. This provides a flexible approach which will improve the accuracy of temperature calculations associated with pile heat exchangers. In particular, including the transient temperature change in the concrete will reduce the range of calculated fluid temperatures, or conversely allow greater energy to be obtained within fixed temperature limits. Thus the proposed new G-functions provide the opportunity for greater efficiency for heat pump systems. In the examples given, this translates to an increase in energy obtained of around 10%. The actual value which will be appropriate for a specific scheme will depend on the details of the pile and ground conditions. However, it will be greater in cases where the piles are of large diameter and the concrete is of low conductivity compared to the surrounding ground.

Acknowledgements

This work has been funded by the Engineering and Physical Sciences Research Council (research grant number EP/H049010/1). The authors would like to thank Nick Woodman for assistance with the Matlab code.

References

- [1] Amis, T. (2009) Geothermal business buoyant, *Geodrilling International*, March 2009, p24.
- [2] Eskilson, P. (1987) *Thermal analysis of heat extraction boreholes*. Doctoral Thesis, Department of Mathematical Physics, University of Lund, Sweden.
- [3] Bandos T. V., Monterob A., Fernández E., Santander J. L. G., Isidroa, J. M. I., Pérez J., Fernández de Córdoba P. J. & Urchueguía J. F. (2009) Finite line-source model for borehole heat exchangers: effect of vertical temperature variations, *Geothermics*, 38, 263 – 270.
- [4] Arup (2005) DTI Partners in Innovation 2002, Ground Storage of Building Heat Energy, Overview Report, PII Ref O-02-ARUP3, May 2005 [Online]. Available at <http://www.arup.com/assets/download/download352.pdf> [accessed 28 May 2012].

- [5] Loveridge, F. & Powrie, W. (2013) Pile heat exchangers: thermal behaviour and interactions, *Proceedings of the Institution of Civil Engineers Geotechnical Engineering*, 166 (2) April 2013, pp tbc. DOI: 10.1680/geng.11.00042
- [6] Ingersoll, L. R., Zobel, O. J. & Ingersoll, A. C. (1954) *Heat Conduction with Engineering and Geological Applications*. 3rd Edition, New York, McGraw-Hill.
- [7] Bernier, M. (2001) Ground Coupled Heat Pump System Simulation, *ASHRAE Transactions*, 107 (1), 605-616
- [8] Loveridge, F., Wood, C. & Powrie, W. (in review) Thermal Response Testing for Pile Heat Exchangers, submitted to *Journal of Geotechnical and Geoenvironmental Engineering*.
- [9] Man, Y., Yang, H., Diao, N., Liu, & Fang, Z. (2010) A new model and analytical solutions for borehole and pile ground heat exchangers, *International Journal of Heat and Mass Transfer*, 53, 253-2601.
- [10] Wood, C. J., Liu, H. & Riffat, S. B. (2010a) An investigation of the heat pump performance and ground temperature of a pile foundation heat exchanger system for a residential building, *Energy*, 35 (12), 3932-4940.
- [11] Wood, C. J., Liu, H. & Riffat, S. B. (2010b) Comparison of a modeled and field tested piled ground heat exchanger system for a residential building and the simulated effect of assisted ground heat recharge, *International Journal of Low Carbon Technologies*, 5 (12), 137-143.
- [12] Loveridge, F. & Powrie, W. (2013) Performance of Piled Foundations Used as Heat Exchangers, *18th International Conference for Soil Mechanics and Geotechnical Engineering*, Paris, France, September 2-5, 2013.
- [13] Loveridge, F. & Powrie, W. (in review) On the thermal resistance of pile heat exchangers. Submitted to *Geothermics*.
- [14] Li, M. & Lai, A. C. K. (2012) new temperature response functions (G-functions) for pile and borehole ground heat exchangers based on composite-medium-line-source theory, *Energy*, 38, 255 – 263.
- [15] Kim, S-K., Bae, G-O., Lee, K-K. & Song, Y. (2010) Field-scale evaluation of the design of borehole heat exchangers for the use of shallow geothermal energy, *Energy*, 35 (2), 2010, 491-500.
- [16] Lee, C.K. & Lam, H.N. (2012) A modified multi-ground-layer model for borehole ground heat exchangers with an inhomogeneous groundwater flow, *Energy*, 47 (1), 378–387.
- [17] Laloui, L., Nuth, M. & Vulliet, L. (2006) Experimental and numerical investigations of the behaviour of heat exchanger pile, *International Journal for Numerical and Analytical Methods in Geomechanics*, 30, 763-781.
- [18] McAdams, W. H. (1942) *Heat Transmission, 2nd edition*. McGraw-Hill, New York.
- [19] Gnielinski, V. (1976). New equation for heat and mass transfer in turbulent pipe and channel flow, *International Chemical Engineering*, 16, 359 – 368.

- [20] Bennet, J., J. Claesson, & G. Hellstrom (1987) *Multipole Method to Compute the Conductive Heat Flow to and between Pipes in A Composite Cylinder*, Notes on Heat Transfer 3-1987, Dep. of Building Technology and Mathematical Physics, Lund Institute of Technology, Sweden.
- [21] Hellstrom, G. (1991) *Ground Heat Storage, Thermal Analysis of Duct Storage Systems, Theory*, Department of Mathematical Physics, University of Lund, Sweden.

Appendix A Curve Fit Results for Ground Temperature Response Functions

The ground temperature response G-function for the upper bound solution for $Fo > 0.1$ takes the form:

$$G_g = a[\ln(Fo)]^7 + b[\ln(Fo)]^6 + c[\ln(Fo)]^5 + d[\ln(Fo)]^4 + e[\ln(Fo)]^3 + f[\ln(Fo)]^2 + g[\ln(Fo)] + h \quad (\text{A-1})$$

where the curve fitting parameters are defined in Table A-1. For $Fo < 0.1$ then G_g should be set to zero.

Table A-1 Curve fitting parameters for upper bound G_g for $0.1 < Fo < 100,000$

	AR=15	AR=25	AR=33	AR=50
a	-4.837×10^{-7}	-3.796×10^{-7}	-2.192×10^{-7}	-5.142×10^{-8}
b	6.597×10^{-6}	6.441×10^{-6}	4.311×10^{-6}	8.756×10^{-7}
c	6.592×10^{-5}	4.129×10^{-5}	2.939×10^{-5}	3.233×10^{-5}
d	-8.843×10^{-4}	-8.687×10^{-4}	-7.328×10^{-4}	-5.292×10^{-4}
e	-4.678×10^{-3}	-3.276×10^{-3}	-2.647×10^{-3}	-2.79×10^{-3}
f	0.03975	0.04415	0.0443	0.04284
g	0.3018	0.3071	0.3076	0.3144
h	0.5715	0.5819	0.5861	0.597
Sum of square errors	4.755×10^{-3}	1.963×10^{-3}	4.36×10^{-3}	3.988×10^{-3}
Coefficient of determination (R^2)	0.99993	0.99998	0.99996	0.99997

The ground temperature response G-function for the lower bound solution for $Fo > 0.25$ takes the form:

$$G_g = a[\ln(Fo)]^7 + b[\ln(Fo)]^6 + c[\ln(Fo)]^5 + d[\ln(Fo)]^4 + e[\ln(Fo)]^3 + f[\ln(Fo)]^2 + g[\ln(Fo)] + h \quad (\text{A-2})$$

where the curve fitting parameters are defined in Table A-2. For $Fo < 0.25$ then G_g should be set to zero.

Table A-2 Curve fitting parameters for lower bound G_g for $0.25 < Fo < 100,000$

	AR=15	AR=25	AR=33	AR=50
a	2.68×10^{-7}	-6.108×10^{-7}	-8.984×10^{-7}	-8.741×10^{-8}
b	-1.306×10^{-5}	1.83×10^{-5}	3.137×10^{-5}	8.243×10^{-6}
c	1.827×10^{-4}	-1.942×10^{-4}	-3.894×10^{-4}	-1.835×10^{-4}
d	-9.15×10^{-5}	1.366×10^{-3}	2.361×10^{-3}	1.894×10^{-3}
e	-0.01434	-0.01275	-0.01257	-0.01375
f	0.05634	0.04932	0.04341	0.04905
g	0.3722	0.3863	0.3928	0.3997
h	0.3989	0.4173	0.4245	0.4267
Sum of square errors	2.332×10^{-3}	4.502×10^{-3}	8.38×10^{-3}	6.404×10^{-3}
Coefficient of determination (R^2)	0.99995	0.99993	0.99989	0.99993

Appendix B Curve Fit Results for Transient Pile Temperature Response Functions

The pile temperature response G-function for $Fo < 10$ takes the form:

$$G_p = a[\ln(Fo)]^6 + b[\ln(Fo)]^5 + c[\ln(Fo)]^4 + d[\ln(Fo)]^3 + e[\ln(Fo)]^2 + f \ln(Fo) + g \quad (\mathbf{B-1})$$

where the curve fitting parameters are defined in Table B-1. For $Fo > 10$ G_p should be set to 1. for $Fo < 0.01$ G_p should be set to zero.

Table B-1 Curve fitting parameters for G_p for $0.01 < Fo < 10$

	Central Pipes		Pipes Near Edge	
	Lower bound	Upper bound	Lower bound	Upper bound
a	-1.005×10^{-4}	3.552×10^{-5}	-1.438×10^{-5}	-2.991×10^{-5}
b	-2.335×10^{-4}	6.017×10^{-5}	1.276×10^{-5}	-8.037×10^{-6}
c	0.003037	-6.033×10^{-4}	9.534×10^{-4}	8.612×10^{-4}
d	0.001803	0.001301	1.307×10^{-4}	-0.001126
e	-0.04339	-0.00744	-0.02446	-0.01086
f	0.1029	0.02559	0.07569	0.04785
g	0.9095	0.9694	0.921	0.939
Sum of square errors	5.11×10^{-4}	4.28×10^{-5}	9.28×10^{-4}	8.96×10^{-5}
Coefficient of determination (R2)	0.99993	0.99995	0.99979	0.99990